Theor Chem Acc (2012) 131:1270
DOI 10.1007/s00214-012-1270-3

REGULAR ARTICLE

On the stability of single-walled carbon nanotubes and their binding strengths

Jakub D. Baran · Wojciech Kołodziejczyk · Peter Larsson · Rajeev Ahuja · J. Andreas Larsson

Received: 1 April 2012 / Accepted: 20 August 2012 / Published online: 12 September 2012

Abstract We have studied the relative stability of hydrogen-terminated single-walled carbon nanotubes (SWNTs) segments, and open-ended SWNT fragments of varying diameter and chirality that are present at the interface of the catalytic metal particles during growth. We have found that hydrogen-terminated SWNTs differ by <1 eV in stability among different chiralities, which presents a challenge for selective and property-controlled growth. In addition, both zigzag and armchair tubes can be the most stable chirality of hydrogen-terminated SWNTs, which is a fundamental obstacle for property-controlled growth utilizing thermodynamic stability. In contrast, the most armchair-like open-ended SWNTs segments are always the most stable ones, followed in sequence by chiral index up to the least stable zigzag segments. We explain the ordering by triple bond stabilization of the carbon dangling bonds at the open ends, which is a fragment stabilization effect that is only manifested when all bonds between two layers are broken. We show convincingly that the bond strength difference between zigzag and armchair tubes is not present when individual bonds are broken or formed.

Keywords Carbon nanotubes · CVD growth · Vapor–liquid–solid mechanism · Density functional theory

J. D. Baran · W. Kołodziejczyk · J. A. Larsson
Tyndall National Institute, University College Cork, Lee Maltings, Prospect Row, Cork, Ireland

Present Address:
J. D. Baran (✉)
Department of Applied Physics, Competence Centre for Catalysis, Chalmers University of Technology, 41296 Göteborg, Sweden
e-mail: jakub.baran@chalmers.se

W. Kołodziejczyk
Department of Physical Chemistry, Wroclaw Medical University, Pl. Nankiera1, 50-140 Wroclaw, Poland

P. Larsson · R. Ahuja
Division of Materials Theory, Department Physics and Astronomy, Uppsala University, Box 516, 751 20 Uppsala, Sweden

1 Introduction

Since their discovery, carbon nanotubes (CNTs) [1] have stimulated a plethora of possible uses because of their high aspect ratio and remarkable mechanical, thermal, optical, and electronic properties [2–7]. Their strength as fibers makes them ideal for the production of strong, but lightweight materials [8]. Their directional [9, 10] thermal transport abilities are second only to diamond, with applications to heat transport in general and as thermal interface material (TIM) for cooling of hotspots in microelectronics applications in particular [11]. Their optical properties have been utilized in field emitters [12–14], and it remains to see what future uses CNTs have in optics and photonics [15]. CNTs can be metallic, semimetallic, or semiconducting, and thus have a range of applications as a naturally nanoshaped material in future semiconductor technology, some of which have been demonstrated in research laboratories, such as nonvolatile memory [16], interconnects [17, 18], and transistor channels [19]. The lower resistivity for metallic CNTs compared to nanosized Cu, and the higher mobility of semiconducting CNTs compared to Si, makes nanotubes a very attractive material. Of particular promise for technological applications are the single-walled carbon nanotubes (SWNTs). They are defined by their diameter and orientation of their internal

graphene hexagonal structure, which can be described by a set of two integers (n and m) called the SWNT index. The internal structuring also determines the electronic properties of the specific tube.

The catalytic chemical vapor deposition (CVD) technique is to date the most reliable production method, but all methods share the same growth mechanism—a modified version of the established vapor–liquid–solid (VLS) mechanism for the production of nanowires [20–24]. The active region of CNT growth is at the interface of the growing CNT and the metal particle that catalyses their growth, that is, tip growth and root growth, only differs in the sense of whether the metal particles are bound to a substrate or not. In order to successfully serve as catalytic centers, metal particles must be able to: (1) decompose the carbon feedstock gas, (2) form graphitic caps at their surface, and (3) stabilize the growing open end to maintain the hollow structure [24, 25], which is required solely because CNTs are hollow. Criteria (1) and (2) share common traits with the VLS growth of nanowires, while (3) is a special feature of CNT growth. Criteria (1)–(3) are only fulfilled by elemental Fe, Co, and Ni [26–30], or their alloys, also with non-catalytic metals, especially Mo [31–33]. In addition, a limited number of studies indicate that some other metals also meet the criteria, for example, Ru [34] and Re [35]. Criterion (3) was recently identified [24] and shown to be fulfilled when the metal–carbon bonds are strong enough to make the dissociation of the catalytic nanoparticle and the SWNT, followed by cap formation of the open nanotube end, unfavorable. Too weak metal–carbon bonds cannot stabilize the open CNT end, which was found to be the case for pure Cu and Au, while Pd was found to be a borderline case [24]. Too strong metal–carbon bonds, on the other hand, would favor the formation of metal carbides over CNTs (e.g., Mo and W). It has been shown, however, that the metal–carbon bonds can be tuned to catalyze CNT growth by mixing weakly bonding metals (Cu or Pd) with strongly bonding metals (Mo or W) [36, 37], effectively proving that Fe, Co, and Ni nanoparticles are not exclusive in their ability to catalyze CNT growth, but merely form bonds with sp^2 nanostructured carbon, which are of the suitable strength.

A growing number of first principles computational studies have been undertaken to better understand CNT growth [24, 25, 36–51]. The introduction of CNTs into technology such as mass-produced nano-interconnects and transistors has been hampered by the fact that CNT production leads to a mixture of CNTs with different properties, and subsequently much effort is being invested in property-controlled SWNT growth, traditionally by aiming for growth of only one type of SWNT by employing schemes that ensure more monodisperse catalytic particles, resulting in a narrow distribution of SWNT diameters. In this study, we report the relative stabilities of SWNTs of similar diameters and reflect on how these energy differences affect this route toward chirality-controlled growth. We have calculated SWNTs and cut them into two pieces, looking at the open-end stability using first principles electronic structure calculations, which means that this work also relates directly to the efforts of re-growth of CNTs from cut nanotube layers, and using cut CNTs as seeds for growth of specific CNTs [52–54]. We have computed binding energies, using density functional theory (DFT), that could serve to improve the parameters for molecular dynamics (MD) force fields [55–58]. We also compare SWNT relative stabilities of both hydrogen-terminated tubes and tube with their ends cut, as it varies according to the tube chirality and draws conclusions regarding the viability of chirality selected growth.

2 Computational details

We have performed full geometry optimizations using density functional theory (DFT) with the generalized gradient approximation (GGA) for the exchange and correlation functional in the PBE formulation [59] utilizing the medium density multigrid ("m4") for exchange–correlation integration and the resolution of identity (RI) approximation, with the atom-centered Gaussian triple-valence polarized basis set "def2-TZVP" for both C and H [60, 61], as implemented in the TURBOMOLE program package [62–64]. Mulliken charges have been computed with the smaller "def2-DZVP" basis set on the PBE/def2-TZVP geometries to avoid the well-known artefacts arising when Mulliken charges are computed with extended basis sets.

All calculations were performed spin polarized in an unrestricted framework. The ferromagnetic ground states were set up as usual (i.e., by spin multiplets with more electrons in alpha shells than beta shells). We did not relax the number of unpaired electrons self-consistently. Instead, a search over possible multiplets was done for each molecule to locate the optimal number of unpaired electrons. Antiferromagnetic singlet states for the hydrogen-terminated SWNTs were constructed using the alpha orbitals from the ferromagnetic solutions as the starting guess orbitals, keeping the same number of unpaired electrons, but arranged antiferromagnetically. We determined the number of spin pairs in the antiferromagnetic states self-consistently by doing single-point calculations with the Vienna ab initio simulation package (VASP) [65–68] using the projector augmented-wave method [69, 70], which allows initialization of one end of the tube one with net spin up and the other end with net spin down. The VASP plane-wave basis set energy cutoff was 500 eV, and a

Gaussian smearing of 0.05 eV was used for partial electronic occupations. The resulting band occupations were always integral or close to integral (>0.99).

Our results on which tubes are antiferromagnetic are consistent between TURBOMOLE and VASP, and the energy difference between the most stable ferromagnetic solution and the antiferromagnetic minimum agree well in all cases but one: the (6,4) tube is found to be most stable in a non-magnetic singlet state with TURBOMOLE, while it is antiferromagnetic in VASP. However, the total energy compared to the most stable ferromagnetic solution is −21 and −32 meV, respectively, that is, the two computational approaches only differ by ca. 10 meV, which is insignificant for the analysis in this work.

3 Results and discussion

3.1 Nanotube segment stabilities

When SWNT growth is initiated on a catalytic metal particle, a cap-formed hemi-fullerene is first formed on the metal surface, after which growth proceeds by carbon addition to the hemi-fullerene edge. Since the edge is chemisorbed to the metal and the inside cap is physisorbed, at one point the inside of the cap will get detached from the metal and a capped tub segment has been formed. This study concerns these tub segments, which we model by replacing the actual caps with simple hydrogen termination of the tubes. In this section, we are concerned with SWNT segments that are hydrogen terminated (capped) in both ends, in order to deduce the pure nanotube properties. We have studied three series of SWNTs with nine, ten, and eleven carbon atoms at each end (18, 20, and 22 carbon atoms per unit cell, which forms layers in the transverse planes perpendicular to the *c*-axis), see, for example, the (5,5) and (10,0) SWNTs of the $(n + m = 10)$ series in Fig. 1. If we index the SWNTs by the (n, m) vector, the $(n + m = 9)$ series consist of five different SWNTs, the (5,4), (6,3), (7,2), (8,1), and (9,0) tubes; the $(n + m = 10)$ and $(n + m = 11)$ series consist of six SWNTs each, namely the (5,5), (6,4), (7,3), (8,2), (9,1), and (10,0) tubes, and the (6,5), (7,4), (8,3), (9,2), (10,1), and (11,0) tubes, respectively. For these nanotubes geometries, we have studied segments with six unit cells, with both ends hydrogen terminated referred to as "*whole*" in the remainder of this work (represented by the (5,5) and (10,0) tubes in Fig. 1), and segments with three unit cells with one end hydrogen terminated and the other end kept open, to model open-ended SWNTs referred to as "*half*" in the remainder of this work (since they represent cutting the six unit cell segments into two identical *halves*). The resulting stoichiometries are $C_{108}H_{18}$ and $C_{54}H_9$ for the $(n + m = 9)$ series, $C_{120}H_{20}$ and $C_{60}H_{10}$ for the $(n + m = 10)$ series, and $C_{132}H_{22}$ and $C_{66}H_{11}$ for the $(n + m = 11)$ series. Using these geometries, we have computed tube-specific carbon dangling bond energies from the cleaving reactions (see below). We have made test calculations with SWNT fragments consisting of eight unit cells and found the carbon dangling bond energy converged to <0.02 eV per bond. It should be noted that the length of the tube fragments is intentionally not converged separately for each tube index, because the aim here is to model the short tube fragments that are initially formed during growth.

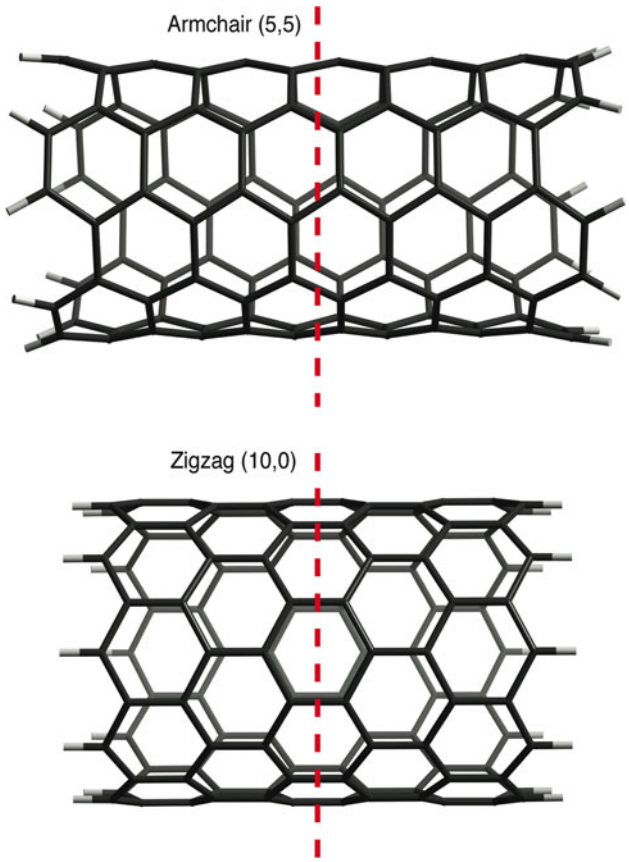

Fig. 1 Molecular structures of hydrogen-terminated single-walled carbon nanotubes (SWNT) segments representative of the *whole* SWNTs used in this study. The *dashed line* represents the cut into *halves* that has been used to calculate open-end stabilities and carbon dangling bond energies. *Top*: (5,5) armchair SWNT, *bottom*: (10,0) zigzag SWNT

We find, analyzing the *whole* hydrogen-terminated SWNT segments, that the total energies do not differ much within a series, as can be seen in Fig. 2. The segments of the $(n + m = 9)$ series are within a 1.37 eV energy window. The corresponding energy window is 0.88 eV and 0.65 eV for the $(n + m = 10)$ and $(n + m = 11)$ series, respectively. The similarity in stability is also reflected in these SWNT's geometric and other energetic properties.

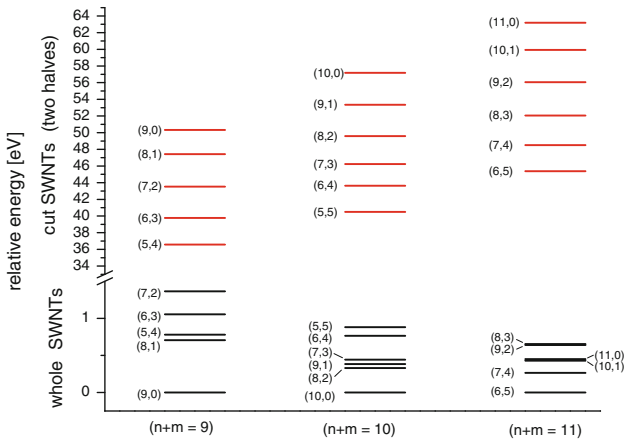

Fig. 2 Bottom part: relative stability of *whole* SWNTs, modeled by hydrogen-terminated six unit cell fragments of the $(n + m = 9)$, $(n + m = 10)$ and $(n + m = 11)$ series (see text). All SWNT energies are compared to the most stable one in each series. Top part: open-ended SWNTs, where each six unit cell tube segment has been cut into two identical *halves* consisting of three unit cells

We find, for example, that the CC bond lengths at the middle section of the *whole* (5,5) SWNT's 1.426 Å, and 1.425 Å for the (10,0) SWNT, which are in practice equal lengths. Similarly, when a single H is removed from the six unit cell (5,5) and (10,0) tubes, the two reaction energies are almost equal at 4.770 and 4.794 eV, respectively. We also note that antiferromagnetic ordering is present in hydrogen-terminated SWNT segments with zigzag character, more specifically the (7,2), (8,1), (9,0), (7,3), (8,2), (9,1), (10,0), (9,2), (10,1), and (11,0) segments. It is in agreement with earlier results [71, 72], which predict antiferromagnetic ground states for the (7,0), (8,0), (9,0), and (10,0) zigzag SWNT segments.

In order to realize chirality-controlled growth, different chiralities must be resolved energetically, but the energy difference between two fundamentally different chiralities, such as (8,1) and (5,4), is typically of the order 0.1 eV, which is close to the thermal energy at growth conditions (1 kT at 1000 K is 0.09 eV). These results show why it is so difficult to achieve chirality-controlled growth of SWNTs, even using almost monodisperse catalytic nanoparticles. It can be directly attributed to the small energetic difference between the different tubes with a fixed number of end atoms at the open (growing) end. In light of these results, it is questionable whether even the same nanoparticle would result in growth of the same SWNT twice (in any larger probability than purely statistical). The energy window, and potential selectivity, of *whole* tubes could possibly be widened by considering larger fragments (as discussed above), but the only way to reach that tube length in practice would be for the tubes to have grown past the length where chirality selection is difficult, by seeding growth with relatively long tube fragments with a specific chirality, which would then have to be obtained by other means, for example, chemical synthesis.

It is interesting to note that different types of SWNTs represent the lower and upper bounds of the energy windows for the three different series. For the $(n + m = 9)$ series, the zigzag (9,0) and most armchair-like (5,4) nanotube are among the most stable ones, while the (7,2) SWNT is the least stable one. For the $(n + m = 10)$ series, the zigzag (10,0) nanotube is also the most stable, but the armchair (5,5) tube is the least stable one. This ordering is completely reversed for the $(n + m = 11)$ series, with the armchair-like (6,5) tube being most stable, and the zigzag-like (9,2) and (8,3) tubes being the least stable ones. Furthermore, the ordering depends on the length of the tube fragments considered. When testing for convergence with respect to the number of unit cells in the fragment, we found that the relative stability in the $(n + m = 9)$ series is different when using eight unit cells compared to six unit cells. It means that the introduction of thermodynamic control of growth would still result in a mixture of metallic and semiconducting SWNTs, even if a very narrow distribution of tube diameters is achieved. Thus, there is a fundamental impediment to growth of only metallic or only semiconducting nanotubes using traditional approaches, which is dictated by SWNT stability.

In addition to variation in the stability of SWNT fragments depending on the length, we find that the electronic properties of the six unit cell SWNT segments differ from those of the corresponding microscopic (or infinite) SWNTs. In Table 1, we report the HOMO–LUMO gaps of the hydrogen-terminated SWNTs segments of the $(n + m = 9)$, $(n + m = 10)$, and $(n + m = 11)$ series. Most are effectively semiconducting at this length. Similar effects have been described elsewhere [71–73].

3.2 Cut nanotube end stabilities

When studying the interface between catalytic metal particles and SWNTs, one always find relatively large

Table 1 Energy gap, ΔE in eV, between the highest occupied molecular orbital (HOMO) and the lowest unoccupied molecular orbital (LUMO) for the six unit cell hydrogen-terminated SWNTs fragments of the $(n + m = 9)$, $(n + m = 10)$ and $(n + m = 11)$ series

$n + m = 9$		$n + m = 10$		$n + m = 11$	
Index	ΔE	Index	ΔE	Index	ΔE
(5,4)	1.49	(5,5)	0.19	(6,5)	1.29
(6,3)	0.93	(6,4)	0.15	(7,4)	0.87
(7,2)	0.37	(7,3)	0.30	(8,3)	0.39
(8,1)	0.49	(8,2)	0.38	(9,2)	0.42
(9,0)	0.66	(9,1)	0.48	(10,1)	0.49
		(10,0)	0.56	(11,0)	0.63

differences in the metal–carbon (M–C) binding energies (BEs) between zigzag and armchair tubes (zigzag tubes have larger M–C BEs in the order of an eV) [24, 25, 48–51]. We investigate how these differences can be reconciled with the relative equal stability of *whole* SWNT segments, and the equality of C–C bond lengths and C–H dissociation energies for zigzag and armchair tubes (as reported above), by considering open-ended nanotube fragments. These were constructed by cutting the hydrogen-terminated tube segments into two identical segments. This approach makes it possible to determine the carbon dangling bond formation energy by simply dividing the total reaction energy by the number of carbon dangling bonds present at the interface.

In contrast to *whole* SWNTs, the energies of two open-ended *half* SWNTs span considerably wider ranges of 13.7 eV, 16.5 eV and 17.8 eV for the $(n + m = 9)$, $(n + m = 10)$ and $(n + m = 11)$ SWNT series (see Fig. 2).

In other words, the open end is much more sensitive to different chiralities. Also in contrast to the situation for *whole* SWNTs, the ordering of the *half* SWNTs is the same for all three series, with the most armchair-like nanotubes [(5,4), (5,5), and (6,5)] being the most stable and the zigzag (least armchair-like) nanotubes [(9,0), (10,0), and (11,0)] being the least stable. One can observe almost incremental increases in energy of 2.9–4.5 eV (1.4–2.2 eV per SWNT end) for each decrease of the second integer of the nanotube index.

The trend in open-end stability with chirality can be explained by carbon dangling bond (DB) stabilization at the cut edges, an effect which is present for both open-ended CNTs and graphene edges [48]. Most importantly, when two DBs are on neighboring carbon atoms, they can pair up in the formation of a partial triple bond, which is the case for all DBs of an armchair tube (see Fig. 3). We have found from our DFT calculations that the optimum number of unpaired electrons at an open end of a SWNT is equal to $u = n–m$, where n and m are the integers of the SWNT index (n and m). Here, the magnetic ordering is always ferromagnetic, which is in agreement with earlier findings [74]. The number of unpaired electrons is an indirect measure of how many DBs pair up into triple bonds for a certain tube index when symmetrically cut (without attempting to cut the tube in an effort to maximize the number of next neighbor DBs of one of the fragments). For the $(n + m = 10)$ series, there can be a maximum of ten unpaired electrons (which is the case for the (10,0) tube), but for, for example, the (7,3) tube six DBs pair up, leaving four unpaired electrons. The presence of triple bonds is also indicated by the resulting C–C bond lengths, which range between 1.243 and 1.250 Å in the armchair sections of cut SWNTs, as compared to the normal partial double bonds of 1.378–1.407 Å in the zigzag sections. Mulliken analysis reveals that there is a small negative

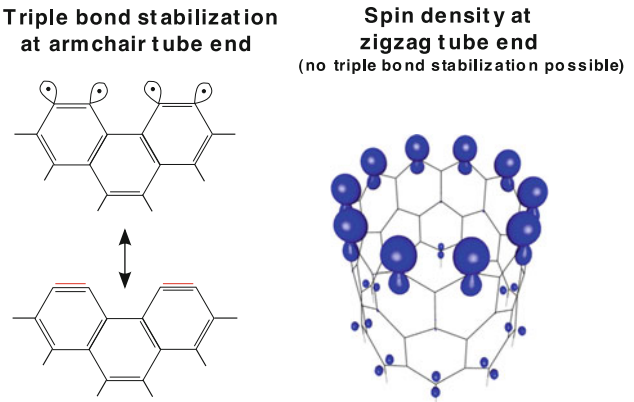

Fig. 3 Fragment stabilization of armchair open ends (*left*) manifested in triple bond formation, which are missing for zigzag open ends (*right*)

charge of −0.1 on both zigzag and armchair open ends, so the partial charge is the same regardless of whether the electrons combine to form triple bonds or are in the form of individual dangling bonds.

Figure 4 shows that DB energies vary from 1.98 eV to 2.85 eV depending on the number of unpaired electrons in an almost linear fashion. This is due to the difference in SWNT edge stabilization discussed above and is thus not directly related to the C–C bond strength at equilibrium [75, 76], that is, the C–C bonds of armchair SWNTs are not weaker (or longer) than those of zigzag SWNTs, but when an armchair SWNT is cut (perpendicular to the long axis), an additional fragment stabilization reduces the DB formation energy compared to zigzag SWNTs. For example, this stabilization effect is not present when only one H atom is removed from the hydrogen-terminated edge of the (5,5) and (10,0) tubes, which results in an almost equal hydrogen removal energy (see above). This tube edge stabilization is the reason behind the differences reported for M–C BEs whether the nanotube is zigzag or armchair. [24, 25, 48–51, 77, 78] It is simply differences in fragment stabilization for one of the dissociation products. And the same deduction can be made for M–C bond strengths as we have made for the C–C ones; any one M–C bond at a zigzag SWNT edge is not stronger than in the case of an armchair edge, but when all bonds or adjacent M–C bonds are broken, an additional fragment stabilization effect reduces the BEs when armchair edge-like partial triple bond formation is possible. Since the dissociation energies between metal particles and SWNT fragments are very large (exceeding 15 eV for the catalytic metals), we recognize that it would be very difficult to utilize chirality-dependent dissociation of armchair-like tubes as a means to achieve chirality-controlled SWNT growth.

Our simulations show that the relative stability between SWNT fragments of different chirality is small for our *whole*

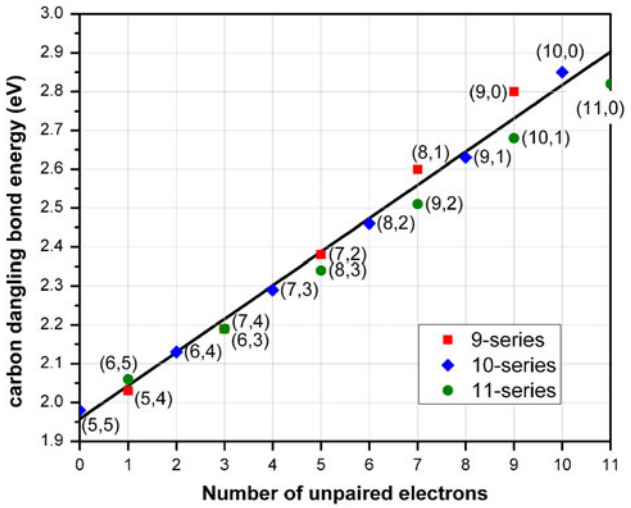

Fig. 4 Carbon dangling bond energies, calculated from the tube dissociation energies divided by the number of carbon dangling bonds versus the optimum number of unpaired electrons for each open-ended *half* SWNT. There is a clear linear relationship between dangling bond energy and number of unpaired electrons

tubes. This is in analogy with the small difference between the (5,5) and (10,0) tube bound to a M_{55} metal cluster, which has been found previously to be only 0.282 eV and 0.799 eV for $M = Co$ and $M = Ni$, respectively [25]. We also show that the difference in *M–C* binding strengths computed for the two extremes armchair and zigzag tubes, which can be as large as 1 eV, is only manifested upon complete dissociation of the tube fragment from the catalytic metal particle. This has been proven by: (1) showing that the difference is mimicked also for the C–C bond strengths obtained from cutting the *whole* tubes into *halves*; (2) explaining the difference to be due to fragment stabilization through triple bond formation of neighboring dangling bonds on simultaneously broken C–C bonds; (3) showing that this difference between the C–C bonds between tube layers is not present for individual bonds. Together, our findings for *whole* tube fragments and for computed binding energies show that the difference in energy between different tube chiralities is small when it comes to practical terms. This means that there is a very limited spectrum for the utilization of relative energy differences between tubes to achieve chirality-controlled SWNT growth. Since the chirality of the tube dictates the tube properties, it is not likely that traditional catalytic CVD techniques will solve the issue of growing only semiconducting or only metallic tubes for different applications.

4 Conclusions

We have studied the relative stability of all possible chiralities of hydrogen-terminated SWNTs segments having 18, 20, and 22 carbon atoms per unit cell; we found that within each series, the total energy of the different chiralities span a range of only 1.4, 0.9, and 0.7 eV, respectively. We relate this finding to relative stabilities between SWNT fragments and catalytic metal particles. Furthermore, for the hydrogen-terminated SWNT segments, both zigzag and armchair tubes can be the most stable chirality for a given diameter. This means that attempts at thermodynamically-controlled growth of a narrow range of tube diameters will result in both metallic and semiconducting tubes. We have investigated the well-known differences between chiralities for open-ended SWNT segments, where the energy difference between two chiralities can be as much as 0.87 eV per carbon dangling bond present at the open end. Our results show that in the case of open-ended SWNT segments, armchair tubes are always the most stable, due to triple bond stabilization of carbon dangling bonds situated on neighboring carbon atoms. The stability of open-ended SWNTs depends on the number of triple bonds that can be formed, which is directly linked to the tube chirality. As a direct consequence, it also governs the number of unpaired electrons at the open end. We relate these results to the reported differences in M–C binding strengths between armchair and zigzag ends/sides of tubes/graphene sheets. However, we find that this difference between chiralities is of very limited use since it is only manifested upon complete cutting of a tube, and in analogy with growth—complete dissociation of the tube from the metal. We show decisively that this difference in C–C/M–C binding strengths between chiralities is not present for individual C–C/M–C bonds.

Acknowledgments The authors are grateful for funding from Intel, Enterprise Ireland, Science Foundation Ireland, and the Marie Curie early stage research training (EST)—NANOCAGE. Calculations were performed at Tyndall National Institute's in-house clusters provided by Science Foundation, Ireland (SFI), at the SFI/HEA Irish Centre for High-End Computing (ICHEC), and at Swedish National Supercomputing facilities.

References

1. Iijima S, Ichihashi T (1993) Single-shell carbon nanotubes of 1-nm diameter. Nature 363(6430):603–605
2. Dresselhaus M, Dresselhaus G, Avouris P (2001) Carbon nanotubes: synthesis, structure. Properties and Applications, Heidelberg
3. Rao CNR, Satishkumar BC, Govindaraj A, Nath M (2001) Nanotubes. ChemPhysChem 2(2):78–105. doi:10.1002/1439-7641(20010216)2:2<78:aid-cphc78>3.0.co;2-7
4. Baughman RH, Zakhidov AA, de Heer WA (2002) Carbon nanotubes—the route toward applications. Science 297(5582): 787–792. doi:10.1126/science.1060928
5. Ebbesen TW, Lezec HJ, Hiura H, Bennett JW, Ghaemi HF, Thio T (1996) Electrical conductivity of individual carbon nanotubes. Nature 382(6586):54–56
6. Wong SS, Woolley AT, Joselevich E, Cheung CL, Lieber CM (1998) Covalently-functionalized single-walled carbon nanotube

probe tips for chemical force microscopy. J Am Chem Soc 120(33): 8557–8558. doi:10.1021/ja9817803
7. Heller I, Kong J, Heering HA, Williams KA, Lemay SG, Dekker C (2004) Individual single-walled carbon nanotubes as nanoelectrodes for electrochemistry. Nano Lett 5(1):137–142. doi:10.1021/nl048200m
8. Breuer O, Sundararaj U (2004) Big returns from small fibers: a review of polymer/carbon nanotube composites. Polym Compos 25(6):630–645. doi:10.1002/pc.20058
9. Schelling PK, Shi L, Goodson KE (2005) Managing heat for electronics. Mater Today 8:30
10. Ivanov I, Puretzky A, Eres G, Wang H, Pan Z, Cui H, Jin R, Howe J, Geohegan DB (2006) Fast and highly anisotropic thermal transport through vertically aligned carbon nanotube arrays. Appl Phys Lett 89(22):223110
11. Kim W, Wang R, Majumdar A (2007) Nanostructuring expands thermal limits. Nano Today 2(1):40–47. doi:10.1016/s1748-0132(07)70018-x
12. Rinzler AG, Hafner JH, Nikolaev P, Lou L, Kim SG, Tomanek D, Nordlander P, Colbert DT, Smalley RE (1995) Unraveling nanotubes—field-emission from an atomic wire. Science 269(5230):1550–1553. doi:10.1126/science.269.5230.1550
13. Deheer WA, Chatelain A, Ugarte D (1995) A carbon nanotube field-emission electron source. Science 270(5239):1179–1180. doi:10.1126/science.270.5239.1179
14. Choi WB, Chung DS, Kang JH, Kim HY, Jin YW, Han IT, Lee YH, Jung JE, Lee NS, Park GS, Kim JM (1999) Fully sealed, high-brightness carbon-nanotube field-emission display. Appl Phys Lett 75(20):3129–3131. doi:10.1063/1.125253
15. Huang Y, Duan X, Lieber CM (2005) Semiconductor nanowire for multi-color photonics. Small 1:142–147
16. Choi WB, Chae S, Bae E, Lee J-W, Cheong B-H, Kim J-R, Kim J–J (2003) Carbon-nanotube-based nonvolatile memory with oxide–nitride–oxide film and nanoscale channel. Appl Phys Lett 82(2):275–277
17. Avouris P, Chen Z, Perebeinos V (2007) Carbon-based electronics. Nat NANO 2(10):605–615
18. Close GF, Yasuda S, Paul B, Fujita S, Wong HSP (2008) A 1 GHz integrated circuit with carbon nanotube interconnects and silicon transistors. Nano Lett 8(2):706–709. doi:10.1021/nl0730965
19. Chaste J, Lechner L, Morfin P, Feve G, Kontos T, Berroir JM, Glattli DC, Happy H, Hakonen P, Placais B (2008) Single carbon nanotube transistor at GHz frequency. Nano Lett 8(2):525–528. doi:10.1021/nl0727361
20. Wagner RS, Ellis WC (1964) Vapor-liquid-solid mechanism of single crystal growth (new method growth catalysis from impurity whisker epitaxial + large crystals si e). Appl Phys Lett 4(5):89. doi:10.1063/1.1753975
21. Baker RTK, Barber MA, Harris PS, Feates FS, Waite RJ (1972) Nucleation and growth of carbon deposits from the nickel catalyzed decomposition of acetylene. J Catal 26(1):51–62. doi:10.1016/0021-9517(72)90032-2
22. Saito Y (1995) Nanoparticles and filled nanocapsules. Carbon 33(7):979–988. doi:10.1016/0008-6223(95)00026-a
23. Rodriguez-Manzo JA, Terrones M, Terrones H, Kroto HW, Sun LT, Banhart F (2007) In situ nucleation of carbon nanotubes by the injection of carbon atoms into metal particles. Nat Nanotechnol 2(5):307–311. doi:10.1038/nnano.2007.107
24. Ding F, Larsson P, Larsson JA, Ahuja R, Duan HM, Rosen A, Bolton K (2008) The importance of strong carbon-metal adhesion for catalytic nucleation of single-walled carbon nanotubes. Nano Lett 8(2):463–468. doi:10.1021/nl072431m
25. Larsson P, Larsson JA, Ahuja R, Ding F, Yakobson BI, Duan HM, Rosen A, Bolton K (2007) Calculating carbon nanotube-catalyst adhesion strengths. Phys Rev B 75(11):115419. doi:10.1103/PhysRevB.75.115419
26. Jung YJ, Homma Y, Ogino T, Kobayashi Y, Takagi D, Wei B, Vajtai R, Ajayan PM (2003) High-density, large-area single-walled carbon nanotube networks on nanoscale patterned substrates. J Phys Chem B 107(28):6859–6864. doi:10.1021/jp0346514
27. Huang SM, Cai XY, Du CS, Liu J (2003) Oriented long single walled carbon nanotubes on substrates from floating catalysts. J Phys Chem B 107(48):13251–13254. doi:10.1021/jp0364708
28. Ciuparu D, Chen Y, Lim S, Haller GL, Pfefferle L (2003) Uniform-diameter single-walled carbon nanotubes catalytically grown in cobalt-incorporated MCM-41. J Phys Chem B 108(2): 503–507. doi:10.1021/jp036453i
29. Kim NS, Lee YT, Park J, Han JB, Choi YS, Choi SY, Choo J, Lee GH (2003) Vertically aligned carbon nanotubes grown by pyrolysis of iron, cobalt, and nickel phthalocyanines. J Phys Chem B 107(35):9249–9255. doi:10.1021/jp034895o
30. Li KinlochIA, Shaffer MSP, Singh C, Geng J, Johnson BFG, Windle AH (2004) Growth of single-walled carbon nanotubes by the rapid heating of a supported catalyst. Chem Mater 16(26): 5637–5643. doi:10.1021/cm0495111
31. Li Y, Liu J, Wang Y, Wang ZL (2001) Preparation of monodispersed Fe–Mo nanoparticles as the catalyst for CVD Synthesis of carbon nanotubes. Chem Mater 13(3):1008–1014. doi:10.1021/cm000787s
32. Wang B, Wei L, Yao L, Li L-J, Yang Y, Chen Y (2007) Pressure-induced single-walled carbon nanotube (n, m) selectivity on co–Mo catalysts. J Phys Chem C 111(40):14612–14616. doi:10.1021/jp0762525
33. Qingwen L, Hao Y, Yan C, Jin Z, Zhongfan L (2002) A scalable CVD synthesis of high-purity single-walled carbon nanotubes with porous MgO as support material. J Mater Chem 12(4):1179–1183
34. Mabudafhasi ML, Bodkin R, Nicolaides CP, Liu XY, Witcomb MJ, Coville NJ (2002) The ruthenium catalysed synthesis of carbon nanostructures. Carbon 40(14):2737–2742. doi:10.1016/s0008-6223(02)00192-6
35. Ritschel M, Leonhardt A, Elefant D, Oswald S, Buchner B (2007) Rhenium-catalyzed growth carbon nanotubes. J Phys Chem C 111(24):8414–8417. doi:10.1021/jp070467x
36. Li Z, Larsson JA, Larsson P, Ahuja R, Tobin JM, O'Byrne J, Morris MA, Attard G, Holmes JD (2008) Copper/molybdenum nanocomposite particles as catalysts for the growth of bamboo-structured carbon nanotubes. J Phys Chem C 112(32):12201–12206. doi:10.1021/jp8023556
37. O'Byrne JP, Li Z, Tobin JM, Larsson JA, Larsson P, Ahuja R, Holmes JD (2010) Growth of carbon nanotubes from heterometallic palladium and copper catalysts. J Phys Chem C 114(18):8115–8119. doi:10.1021/jp909309t
38. Yazyev OV, Pasquarello A (2008) Effect of metal elements in catalytic growth of carbon nanotubes. Phys Rev Lett 100(15): 156102
39. Fan X, Buczko R, Puretzky AA, Geohegan DB, Howe JY, Pantelides ST, Pennycook SJ (2003) Nucleation of single-walled carbon nanotubes. Phys Rev Lett 90(14):145501
40. Lee YH, Kim SG, Tomnek D (1997) Catalytic growth of single-wall carbon nanotubes: an ab initio study. Phys Rev Lett 78(12):2393–2396
41. Charlier J-C, De Vita A, Blase X, Car R (1997) Microscopic growth mechanisms for carbon nanotubes. Science 275(5300): 647–649. doi:10.1126/science.275.5300.647
42. Gavillet J, Loiseau A, Journet C, Willaime F, Ducastelle F, Charlier JC (2001) Root-growth mechanism for single-wall carbon nanotubes. Phys Rev Lett 87(27):275504
43. Raty J-Y, Fo Gygi, Galli G (2005) Growth of carbon nanotubes on metal nanoparticles: a microscopic mechanism from ab initio molecular dynamics simulations. Phys Rev Lett 95(9):096103

44. Reich S, Li L, Robertson J (2006) Control the chirality of carbon nanotubes by epitaxial growth. Chem Phys Lett 421(4–6): 469–472. doi:10.1016/j.cplett.2006.01.110
45. Reich S, Li L, Robertson J (2005) Structure and formation energy of carbon nanotube caps. Phys Rev B 72(16):165423
46. Helveg S, Lopez-Cartes C, Sehested J, Hansen PL, Clausen BS, Rostrup-Nielsen JR, Abild-Pedersen F, Norskov JK (2004) Atomic-scale imaging of carbon nanofibre growth. Nature 427(6973):426–429. doi:http://www.nature.com/nature/journal/v427/n6973/suppinfo/nature02278_S1.html
47. Shin Y-H, Hong S (2008) Carbon diffusion around the edge region of nickel nanoparticles. Appl Phys Lett 92(4):043103
48. Liu Y, Dobrinsky A, Yakobson BI (2010) Graphene edge from armchair to zigzag: the origins of nanotube chirality? Phys Rev Lett 105(23):235502
49. Dumlich H, Reich S (2010) Chirality-dependent growth rate of carbon nanotubes: a theoretical study. Phys Rev B 82(8):085421
50. Borjesson A, Bolton K (2011) Modeling of ostwald ripening of metal clusters attached to carbon nanotubes. J Phys Chem C 115(50):24454–24462. doi:10.1021/jp202328w
51. Ding F, Harutyunyan AR, Yakobson BI (2009) Dislocation theory of chirality-controlled nanotube growth. Proc Nat Acad Sci 106(8):2506–2509. doi:10.1073/pnas.0811946106
52. Wang Y, Kim MJ, Shan H, Kittrell C, Fan H, Ericson LM, Hwang W-F, Arepalli S, Hauge RH, Smalley RE (2005) Continued growth of single-walled carbon nanotubes. Nano Lett 5(6):997–1002. doi:10.1021/nl047851f
53. Smalley RE, Li Y, Moore VC, Price BK, Colorado R, Schmidt HK, Hauge RH, Barron AR, Tour JM (2006) Single wall carbon nanotube amplification: en route to a type-specific growth mechanism. J Am Chem Soc 128(49):15824–15829. doi:10.1021/ja065767r
54. Iwasaki T, Robertson J, Kawarada H (2008) Mechanism analysis of interrupted growth of single-walled carbon nanotube arrays. Nano Lett 8(3):886–890. doi:10.1021/nl073119f
55. Bolton K, Ding F, Rosén A (2011) Atomistic simulations of catalyzed carbon nanotube growth. J Nanosci Nanotechnol 6(5):1211–1224. doi:10.1166/jnn.2006.145
56. Ding F, Bolton K, Rosén A (2004) Nucleation and growth of single-walled carbon nanotubes: a molecular dynamics study. J Phys Chem B 108(45):17369–17377. doi:10.1021/jp046645t
57. Duan H, Ding F, Rosén A, Harutyunyan A, Tokune T, Curtarolo S, Bolton K (2007) Initial growth of single-walled carbon nanotubes on supported iron clusters: a molecular dynamics study. Eur Phys J D Atomic Mol Opt Plasma Phys 43(1):185–189. doi:10.1140/epjd/e2007-00109-6
58. Maruyama S, Shibuta Y (2002) Molecular dynamics in formation process of SWNTs. Mol Cryst Liquid Cryst 387:311–316. doi:10.1080/10587250290113592
59. Perdew JP, Burke K, Ernzerhof M (1996) Generalized gradient approximation made simple. Phys Rev Lett 77(18):3865
60. Schafer A, Huber C, Ahlrichs R (1994) Fully optimized contracted gaussian-basis sets of triple zeta valence quality for atoms li to kr. J Chem Phys 100(8):5829–5835
61. Weigend F, Ahlrichs R (2005) Balanced basis sets of split valence, triple zeta valence and quadruple zeta valence quality for H to Rn: design and assessment of accuracy. Phys Chem Chem Phys 7(18):3297–3305
62. Treutler O, Ahlrichs R (1995) Efficient molecular numerical-integration schemes. J Chem Phys 102(1):346–354. doi:10.1063/1.469408
63. Von Arnim M, Ahlrichs R (1998) Performance of parallel TURBOMOLE for density functional calculations. J Comput Chem 19(15):1746–1757. doi:10.1002/(sici)1096-987x(19981130)19:15<1746:aid-jcc7>3.3.co;2-m
64. Eichkorn K, Treutler O, Öhm H, Häser M, Ahlrichs R (1995) Auxiliary basis sets to approximate coulomb potentials. Chem Phys Lett 242(6):652–660
65. Kresse G, Hafner J (1993) Ab initio molecular dynamics for liquid metals. Phys Rev B 47(1):558–561
66. Kresse G, Hafner J (1994) Ab initio molecular-dynamics simulation of the liquid-metal, amorphous-semiconductor transition in germanium. Phys Rev B 49(20):14251–14269
67. Kresse G, Furthmuller J (1996) Efficiency of ab initio total energy calculations for metals and semiconductors using a plane-wave basis set. Comput Mater Sci 6(1):15–50. doi:10.1016/0927-0256(96)00008-0
68. Kresse G, Furthmuller J (1996) Efficient iterative schemes for ab initio total-energy calculations using a plane-wave basis set. Phys Rev B 54(16):11169–11186
69. Blöchl PE (1994) Projector augmented-wave method. Phys Rev B 50(24):17953–17979
70. Kresse G, Joubert D (1999) From ultrasoft pseudopotentials to the projector augmented-wave method. Phys Rev B 59(3):1758–1775
71. Hod O, Scuseria GE (2008) Half-metallic zigzag carbon nanotube dots. ACS Nano 2(11):2243–2249. doi:10.1021/nn8004069
72. Hod O, Peralta JE, Scuseria GE (2007) Edge effects in finite elongated graphene nanoribbons. Phys Rev B 76(23):233401
73. Rochefort A, Salahub DR, Avouris P (1999) Effects of finite length on the electronic structure of carbon nanotubes. J Phys Chem B 103(4):641–646. doi:10.1021/jp983725m
74. Kim Y-H, Choi J, Chang KJ, Tomnek D (2003) Defective fullerenes and nanotubes as molecular magnets: An ab initio study. Phys Rev B 68(12):125420
75. Cremer D, Wu A, Larsson A, Kraka E (2000) Some thoughts about bond energies, bond lengths, and force constants. J Mol Model 6(4):396–412. doi:10.1007/pl00010739
76. Larsson JA, Cremer D (1999) Theoretical verification and extension of the McKean relationship between bond lengths and stretching frequencies. J Mol Struct 485–486(0):385–407. doi:10.1016/s0022-2860(99)00093-9
77. Yoshida H, Takeda S, Uchiyama T, Kohno H, Homma Y (2008) Atomic-scale in situ observation of carbon nanotube growth from solid state iron carbide nanoparticles. Nano Lett 8(7):2082–2086. doi:10.1021/nl080452q
78. Page AJ, Ohta Y, Irle S, Morokuma K (2010) Mechanisms of single-walled carbon nanotube nucleation, growth, and healing determined using QM/MD methods. Acc Chem Res 43(10): 1375–1385. doi:10.1021/ar100064g